J. Fluid Mech. (1993), *vol.* 246, *pp.* 21–41

Three-dimensional boundary-layer instability and separation induced by small-amplitude streamwise vorticity in the upstream flow

By M. E. GOLDSTEIN[1] AND S. J. LEIB[2]

[1]NASA Lewis Research Center, Cleveland, OH 44135, USA

[2]Sverdrup Technology, Inc., Lewis Research Center Group, Cleveland, OH 44135, USA

(Received 27 January 1992 and in revised form 25 June 1992)

We consider the effects of a small-amplitude, steady, streamwise vorticity field on the flow over an infinitely thin flat plate in an otherwise uniform stream. We show how the initially linear perturbation, ultimately leads to a small-amplitude but nonlinear cross-flow far downstream from the leading edge. This motion is imposed on the boundary-layer flow and eventually causes the boundary layer to separate. The streamwise velocity profiles within the boundary layer become inflexional in localized spanwise regions just upstream of the separation point. The flow in these regions is therefore susceptible to rapidly growing inviscid instabilities.

1. Introduction

Experimentalists have obtained a great deal of information about laminar boundary layers by studying the flows over relatively thin flat plates embedded in nominally uniform free streams. Such experiments are attempts to simulate the flow over an infinitely thin flat plate embedded in a completely uniform stream and it is important to know how relatively small imperfections in the experimental environment can change the final measured results.

Goldstein, Leib & Cowley (1992, hereinafter referred to as I), showed how small (but steady) spanwise variations in the incident streamwise velocity field can produce somewhat larger streamwise vorticity fields within the boundary layer which can, in turn, produce significant (i.e. order-one) variations in the streamwise velocity profiles. In fact the alterations in the boundary-layer motion ultimately become large enough to separate the flow. Inviscid vortex stretching in the main stream causes the separation to develop relatively close to the leading edge and a fairly complete analytical description of the separation structure was then obtained. This separation, which is of the boundary-layer collision type (Stewartson, Cebeci & Chang 1980; Stewartson & Simpson 1982), occurs on a symmetry plane and the wall shear stress was shown to vanish at the separation point. However, the streamwise velocity profiles were completely non-inflexional.

Here we consider the case where the upstream vorticity is entirely in the streamwise direction so that there is no vortex stretching resulting from the potential flow over the plate. The effects of plate thickness are then largely irrelevant and the pertinent physics are best elucidated by considering the flow over an infinitely thin flat plate. The resulting flow fields (both inside and outside the boundary layer) are now quite different from those in I. In fact the separation now occurs much further downstream than before and is moved off the symmetry plane by a moderately

strong secondary vortex induced by the external inviscid vorticity field. The present study is therefore complementary to that of I and the two taken together provide a more or less complete description of the phenomena that occur in slightly non-uniform flows over two-dimensional flat plates.

As in I, we assume that

$$R_\lambda \gg 1/\epsilon, \tag{1.1}$$

where R_λ is the Reynolds number based on the characteristic lengthscale λ of the upstream disturbance field and ϵ denotes the characteristic amplitude of that disturbance (relative to the undisturbed free-stream velocity field). The upstream distortion again interacts linearly with the leading edge with the resulting flow being well described by the usual 'rapid distortion' theory (Hunt & Carruthers 1990; Goldstein 1978). However, the absence of vortex stretching now precludes the important logarithmic singularity that dominates the near-wall flow in I.

The inviscid cross-flow effects again produce only a linear perturbation of the boundary-layer flow in the vicinity of the leading edge, where the undisturbed boundary layer undergoes its most rapid streamwise development, but they produce an order-one change in the mean boundary layer profiles at large distances downstream where the boundary layer develops on a considerably longer scale. The linear rapid distortion theory solution again breaks down at large streamwise distances from the leading edge (even though the cross-flow velocities remain small) and a new nonlinear solution has to be obtained in order to describe the inviscid flow outside the boundary layer in the physically interesting region where cross-flow effects produce significant (i.e. order-one) profile changes in that layer. However, the nonlinear region now occurs somewhat further downstream and the resulting inviscid flow is described by the two-dimensional time-dependent inviscid vorticity equation (with the streamwise coordinate playing the role of the time) rather than by the inviscid Burgers' equation that was obtained in I. The associated boundary-layer flow is therefore quite different from that found in I, with the streamwise velocity profiles now becoming inflexional before the boundary layer separates. The separation is again of the boundary-layer collision type but, as already indicated, is moved off the symmetry plane by a secondary streamwise vortex.

The inflexional velocity profiles occur just upstream of the separation point and, as anticipated by Prandtl (1935) over fifty years ago, arise from the counter-rotating streamwise vortices in the boundary layer which result from the streamwise vorticity imposed on the flow. These profiles are, as Prandtl (1935) suggested (see also Hall & Horseman 1991), unstable to Rayleigh instabilities which grow on a streamwise lengthscale on the order of the boundary-layer thickness and can therefore dominate the much slower growing Tollmien–Schlichting waves, which are the only instability that would exist in the absence of streamwise vorticity. Our calculations show that the Rayleigh instabilities exhibit large growth and can therefore lead to a local transition of the boundary layer before it is able to separate. The resulting turbulent flow would probably resemble a turbulent spot which, in the real flow, is likely to move around on the surface because the imposed streamwise vorticity would not be very steady in any realistic experiment. This phenomenon might therefore resemble a kind of 'bypass transition' that is sometimes observed in the laboratory. (The term 'bypass transition' is currently used to denote any transition process which circumvents the relatively slow process of Tollmien–Schlichting wave linear growth, non-linear interaction, three-dimensional development and so on to fully developed turbulence.) Of course the Tollmien–Schlichting waves can begin their growth well

upstream of where the streamwise profiles become inflexional and therefore lead to transition before the latter can occur.

The present three-dimensional boundary-layer flow bears some resemblance to the Görtler vortex flows considered by Hall (1988). The primary difference is that the streamwise vortices reside in the outer inviscid flow in the present analysis and can therefore persist over long streamwise distances without the aid of surface curvature effects to counteract the streamwise decay that would otherwise occur. Görtler vortices reside within the boundary layer and exhibit streamwise growth as a result of the surface curvature effects. It might appear on the face of it that our analysis should reduce to that of Hall (1988) when surface curvature effects are included and the disturbance Reynolds number ϵR_λ is allowed to approach unity. However, Crow (1966) considered the $O(1)$ disturbance Reynolds number case with zero curvature and showed that the viscous effects are no longer confined to the boundary layer in this limit, as they are in the Hall (1988) analysis. The present small-disturbance Reynolds number scaling allows free-stream disturbances to become fully nonlinear before viscous effects can set in. This, in turn, has an important effect on the subsequent development of the flow and leads to an asymptotic solution that exhibits some interesting features of the motion which would otherwise be obscured by viscous phenomena.

The present study also bears some resemblance to the receptivity analyses of Goldstein (1983, 1985), Goldstein, Sockol & Sanz (1983) and Goldstein, Leib & Cowley (1987) in that it involves the internalization of free-stream disturbances with an attendant streamwise amplification of the perturbed boundary-layer flow, but it differs from them in that it only involves changes in the mean flow and does not depend on the growth of local instability waves to produce the final effect. More recent studies of Hall (1990) that consider the receptivity issue for Görtler vortices are more closely related to the present analysis. An important difference is that Hall's (1990) input disturbance is imposed at the leading (upstream) edge of the boundary layer whereas (as in Goldstein 1983) the present analysis imposes the disturbance far upstream of the leading edge where the flow is uninfluenced by the plate. We believe that this type of input better characterizes the experimental configurations since it allows the disturbance to be specified independently of surface geometry effects. Indeed it is only by specifying the disturbance in this way that inviscid interaction effects with the solid surface, such as the vortex stretching considered in I, can be accounted for. The fundamental differences between the present results and those of I are ample testimony that such effects must be accounted for in order to properly predict the experimental results. The exact variation of the disturbance in the direction normal to the plate seems to be relatively unimportant and should not effect the results qualitatively. (We note in this regard that Hall 1990 takes the imposed disturbance to be periodic in this direction while we ultimately allow it to decay exponentially.)

The overall plan of the paper is as follows. In §2 the problem is formulated and the linear inviscid flow solutions produced by the steady upstream distortion field and its subsequent breakdown are discussed. The appropriate nonlinear inviscid solution that eliminates the breakdown is described in §3. The viscous boundary-layer problem is formulated in §4. The numerical procedures for calculating both the nonlinear inviscid flow and the three-dimensional boundary-layer flow are discussed in §5. The numerical results, corresponding to a relatively simple choice of the upstream disturbance, are discussed in §6.

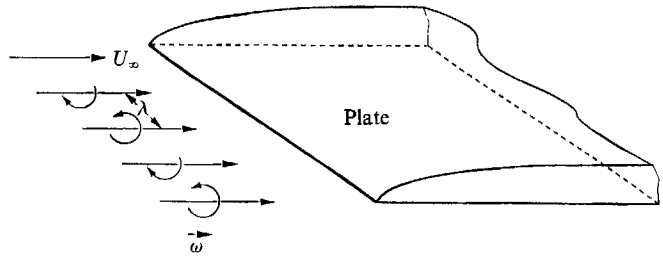

FIGURE 1. Problem geometry.

2. Formulation and breakdown of the linear solution

We are concerned with the flow over a semi-infinite flat plate due to a small, $O(\epsilon)$ streamwise vorticity field, with characteristic lengthscale λ, imposed on an otherwise uniform upstream flow (see figure 1). We suppose that the flow is incompressible, that all lengths are normalized by λ, that the velocity $\boldsymbol{u} = \{u, v, w\}$ has been normalized by the uniform upstream velocity U_∞ and that the pressure has been normalized by ρU_∞^2, where ρ is the (constant) density. We take the origin of the $\{x, y, z\}$ coordinate system to be at the leading edge of the plate with x in the streamwise direction and y normal to the plate.

It follows that

$$\boldsymbol{u} \to \left\{1, \epsilon\frac{\partial \psi_\infty}{\partial z}, -\epsilon\frac{\partial \psi_\infty}{\partial y}\right\} \quad \text{as} \quad x \to -\infty, \tag{2.1}$$

where $\psi_\infty = \psi_\infty(y, z)$ is a cross-flow stream function that can be used to characterize the upstream disturbance.

The effects of plate thickness are largely irrelevant and we suppose, for simplicity, that the plate is infinitely thin. Finally the Reynolds number $R_\lambda = U_\infty \lambda/\nu$, where ν is the kinematic viscosity, is assumed to be large enough so that viscous effects are initially confined to a thin boundary layer near the surface of the plate.

2.1. *The linear solution*

The non-uniform flow outside the boundary layer is governed by linear rapid distortion theory in the vicinity of the leading edge, i.e. where $x = O(1)$. The boundary-layer flow below this region is nearly two-dimensional with three-dimensional effects being only an $O(\epsilon)$ perturbation of this otherwise Blasius flow. The inviscid solution should therefore expand like

$$\begin{aligned}\boldsymbol{u} &= \{1,0,0\} + \epsilon\{u_0, v_0, w_0\} + \epsilon^2\{u_1, v_1, w_1\} + \ldots \\ &= \{1,0,0\} + \epsilon u_0 + \epsilon^2 u_1 + \ldots, \end{aligned} \tag{2.2}$$

$$p = \epsilon p_0 + \epsilon^2 p_1 + \ldots. \tag{2.3}$$

The zeroth-order terms are governed by the linearized Euler equations and the results given in Goldstein (1978) can be used to write this as

$$\boldsymbol{u}_0 = \nabla\phi + \hat{\boldsymbol{j}}\frac{\partial \psi_\infty}{\partial z} - \hat{\boldsymbol{k}}\frac{\partial \psi_\infty}{\partial y}, \tag{2.4}$$

and

$$p_0 = -\partial\phi/\partial x, \tag{2.5}$$

where ϕ can be determined from

$$\nabla^2\phi = 0, \tag{2.6}$$

subject to the boundary conditions

$$\phi(x,0^+,z)=\phi(x,0^-,z), \quad x<0; \quad \frac{\partial\phi}{\partial y}=-\frac{\partial\psi_\infty}{\partial z}, \quad y=0, x>0, \tag{2.7}$$

with $\hat{\boldsymbol{j}}$ and $\hat{\boldsymbol{k}}$ being the unit vectors in the y- and z-directions, respectively.

2.2. *Breakdown of the linear solution*

The linear inviscid problem (2.6) and (2.7) can be solved by the Wiener–Hopf technique (Nobel 1958). We note in passing that the relevant solution has a 'square root' singularity at the leading edge of the plate but this has no effect on our analysis – provided, of course, that massive separation does not occur. This is because the boundary layer would, at most, be locally three-dimensional in the vicinity of the leading edge and would return to a predominantly two-dimensional Blasius flow well upstream of the nonlinear region that is of primary interest herein. Of course, all real flat plates have blunt leading edges which preclude the occurrence of a singularity in any real flow. We can then, if necessary, suppose that the leading-edge radius is large enough to prevent the occurrence of separation, but still small enough to be consistent with the infinitely thin flat plate model in so far as it effects the downstream flow. The results show that ϕ becomes independent of x as $x\to\infty$ and, in view of (2.4) and (2.5), that

$$u_0, p_0 \to 0 \quad \text{as} \quad x\to\infty. \tag{2.8}$$

It follows that the downstream motion, like the upstream flow, is basically two-dimensional and can therefore be determined from a single cross-flow stream function

$$\psi_0=\psi_0(y,z), \tag{2.9}$$

such that

$$\boldsymbol{u}_0 \to \left\{0, \frac{\partial\psi_0}{\partial z}, -\frac{\partial\psi_0}{\partial y}\right\} \quad \text{as} \quad x\to\infty. \tag{2.10}$$

However, this solution is non-uniformly valid as $x\to\infty$. To show this we note that the first-order solution satisfies

$$\frac{\partial\boldsymbol{u}_1}{\partial x}+\nabla p_1=-\boldsymbol{u}_0\cdot\nabla\boldsymbol{u}_0$$

$$\to \hat{\boldsymbol{j}}\frac{\partial(\psi_0,\psi_{0z})}{\partial(y,z)}-\hat{\boldsymbol{k}}\frac{\partial(\psi_0,\psi_{0y})}{\partial(y,z)} \quad \text{as} \quad x\to\infty \tag{2.11}$$

and

$$\nabla\cdot\boldsymbol{u}_1=0. \tag{2.12}$$

It follows that

$$\nabla^2 p_1 \to \frac{\partial}{\partial y}\frac{\partial(\psi_0,\psi_{0z})}{\partial(y,z)}-\frac{\partial}{\partial z}\frac{\partial(\psi_0,\psi_{0y})}{\partial(y,z)}=2(\psi_{0yy}\psi_{0zz}-\psi_{0zz}^2) \quad \text{as} \quad x\to\infty \tag{2.13}$$

and therefore that p_1 can only vanish at $y=\infty$ if it becomes independent of x as $x\to\infty$, i.e.

$$p_1\to p_\infty(y,z) \quad \text{as} \quad x\to\infty. \tag{2.14}$$

Equation (2.11) now shows that

$$v_1 \to \left[\frac{\partial(\psi_0,\psi_{0z})}{\partial(y,z)}-p_{\infty y}\right]x \tag{2.15}$$

and
$$w_1 \to -\left[\frac{\partial(\psi_0, \psi_{0y})}{\partial(y,z)} + p_{\infty z}\right] x \tag{2.16}$$

as $x \to \infty$, which implies that the zeroth- and first-order solutions become of the same order when
$$\bar{x} \equiv \epsilon x = O(1). \tag{2.17}$$

3. Nonlinear inviscid solution

To obtain the solution in this region we introduce the scaled streamwise variable (2.17) into the Navier–Stokes equations and, in view of (2.2) and (2.8), seek solutions of the form
$$u = 1 + \epsilon^2 \tilde{u}_0 + \ldots, \tag{3.1}$$
$$v = \epsilon \tilde{v}_0 + \ldots, \tag{3.2}$$
$$w = \epsilon \tilde{w}_0 + \ldots, \tag{3.3}$$
$$p = \epsilon^2 \tilde{p}_0 + \ldots. \tag{3.4}$$

It follows from (1.1) that the viscous terms, which are now $O(\epsilon/R_\lambda)$, are still negligible compared to the inviscid terms, which are $O(\epsilon^2)$, and therefore that
$$\left(\frac{\partial}{\partial \bar{x}} + \tilde{v}_0 \frac{\partial}{\partial y} + \tilde{w}_0 \frac{\partial}{\partial z}\right) \tilde{u}_0 = -\frac{\partial \tilde{p}_0}{\partial \bar{x}}, \tag{3.5}$$
$$\left(\frac{\partial}{\partial \bar{x}} + \tilde{v}_0 \frac{\partial}{\partial y} + \tilde{w}_0 \frac{\partial}{\partial z}\right) \tilde{v}_0 = -\frac{\partial \tilde{p}_0}{\partial y}, \tag{3.6}$$
$$\left(\frac{\partial}{\partial \bar{x}} + \tilde{v}_0 \frac{\partial}{\partial y} + \tilde{w}_0 \frac{\partial}{\partial z}\right) \tilde{w}_0 = -\frac{\partial \tilde{p}_0}{\partial z}, \tag{3.7}$$
$$\frac{\partial \tilde{v}_0}{\partial y} + \frac{\partial \tilde{w}_0}{\partial z} = 0. \tag{3.8}$$

Equation (3.8) shows that we can again introduce a cross-flow stream function, say $\tilde{\psi}_0(\bar{x}, y, z)$, such that
$$\tilde{v}_0 = \frac{\partial \tilde{\psi}_0}{\partial z} \tag{3.9}$$

and
$$\tilde{w}_0 = -\frac{\partial \tilde{\psi}_0}{\partial y}. \tag{3.10}$$

Inserting this in (3.6) and (3.7), and eliminating the pressure in the usual way, we obtain
$$\left(\frac{\partial}{\partial \bar{x}} + \tilde{v}_0 \frac{\partial}{\partial y} + \tilde{w}_0 \frac{\partial}{\partial z}\right) \nabla_T^2 \tilde{\psi}_0 = 0, \tag{3.11}$$

or, equivalently
$$\frac{\partial}{\partial \bar{x}} \nabla_T^2 \tilde{\psi}_0 - \frac{\partial(\tilde{\psi}_0, \nabla_T^2 \tilde{\psi}_0)}{\partial(y,z)} = 0, \tag{3.12}$$

where
$$\nabla_T^2 \equiv \frac{\partial^2}{\partial y^2} + \frac{\partial^2}{\partial z^2}, \tag{3.13}$$

is the transverse Laplacian. This equation is just the two-dimensional time-dependent vorticity equation with the scaled streamwise coordinate $\bar{x}$ playing the role of the time. Equations (2.2), (2.8), (3.2), (3.3), (3.9) and (3.10) show that its solutions will match with the linear solution of the previous section if we require that
$$\tilde{\psi}_0 = \psi_0(y,z) \quad \text{at} \quad \bar{x} = 0, \tag{3.14}$$

and the normal velocity will vanish at the plate if we require that

$$\frac{\partial \tilde{\psi}_0}{\partial z} = 0 \quad \text{at} \quad y = 0 \quad \text{for} \quad \bar{x} \geqslant 0. \tag{3.15}$$

These conditions, along with the requirement that $\tilde{\psi}_0 \to 0$ as $y \to \infty$, uniquely determine the solution to (3.12).

4. The viscous boundary layer

Viscous effects must, of course, come into play when y becomes sufficiently small. This occurs when

$$\bar{y} \equiv y/\delta = O(1), \tag{4.1}$$

where

$$\delta \equiv (L/\lambda) R^{-\frac{1}{2}} \tag{4.2}$$

and

$$R \equiv U_\infty L/\nu, \tag{4.3}$$

are the boundary-layer thickness and Reynolds number, respectively, based on the long streamwise lengthscale

$$L = \lambda/\epsilon \tag{4.4}$$

associated with the nonlinear inviscid region.

The streamwise velocity

$$u = U(\bar{x}, \bar{y}, z) + \ldots, \tag{4.5}$$

must be of order one and the requirements of continuity suggest that the scaled cross-flow velocities V and W will be order one if we put

$$v = \epsilon\delta V(\bar{x}, \bar{y}, z) + \ldots, \tag{4.6}$$

$$w = \epsilon W(\bar{x}, \bar{y}, z) + \ldots. \tag{4.7}$$

Equation (3.4) implies that the pressure will scale like

$$p = \epsilon^2 P(\bar{x}, z) + \ldots, \tag{4.8}$$

where P is, of course, of order one.

Substituting these into the full Navier–Stokes equations we obtain the three-dimensional boundary-layer equations

$$U\frac{\partial U}{\partial \bar{x}} + V\frac{\partial U}{\partial \bar{y}} + W\frac{\partial U}{\partial z} = \frac{\partial^2 U}{\partial \bar{y}^2}, \tag{4.9}$$

$$U\frac{\partial W}{\partial \bar{x}} + V\frac{\partial W}{\partial \bar{y}} + W\frac{\partial W}{\partial z} = -\frac{\partial P}{\partial z} + \frac{\partial^2 W}{\partial \bar{y}^2}, \tag{4.10}$$

$$\frac{\partial U}{\partial \bar{x}} + \frac{\partial V}{\partial \bar{y}} + \frac{\partial W}{\partial z} = 0. \tag{4.11}$$

The zero-slip condition implies that

$$U = V = W = 0 \quad \text{at} \quad \bar{y} = 0, \tag{4.12}$$

and in order to match with (3.1)–(3.4) we must require that

$$U \to 1, \quad W \to \tilde{w}_0(\bar{x}, 0, z) \quad \text{as} \quad \bar{y} \to \infty, \tag{4.13}$$

and

$$P = \tilde{p}_0(\bar{x}, 0, z). \tag{4.14}$$

Then, since the cross-flow effects become small as $\bar{x} \to 0$, U must go to the Blasius solution in this limit, i.e.

$$U \to U_B(\bar{x}, \bar{y}) \quad \text{as} \quad \bar{x} \to 0. \tag{4.15}$$

5. Numerical methods

In this section we describe the numerical methods used to solve the nonlinear inviscid and viscous problems obtained in §§3 and 4, respectively.

5.1. *The nonlinear inviscid flow*

The nonlinear inviscid flow must be determined by numerically solving (3.12)–(3.16). To this end we write (3.12) in the 'vorticity–stream function' form as

$$\frac{\partial \tilde{\Omega}_0}{\partial \bar{x}} + \tilde{v}_0 \frac{\partial \tilde{\Omega}_0}{\partial y} + \tilde{w}_0 \frac{\partial \tilde{\Omega}_0}{\partial z} = 0, \tag{5.1}$$

with

$$\nabla_T^2 \tilde{\psi}_0 = \tilde{\Omega}_0. \tag{5.2}$$

The calculations are carried out for a disturbance that is periodic in the spanwise direction, so it is appropriate to introduce the Fourier expansion

$$\tilde{\psi}_0(\bar{x}, y, z) = \sum_{n=-N}^{N} \tilde{\psi}_0^n(\bar{x}, y)\, e^{inz}, \tag{5.3}$$

with

$$\tilde{\psi}_0^{-n} = \tilde{\psi}_0^{n*}, \tag{5.4}$$

where $*$ represents the complex conjugate, etc. into (5.1) and (5.2) to obtain

$$\frac{\partial \tilde{\Omega}_0^n}{\partial \bar{x}} + \sum_{m=-N}^{N} im\tilde{w}_0^{n-m} \tilde{\Omega}_0^m + \sum_{m=-N}^{N} \tilde{v}_0^{n-m} \frac{\partial \tilde{\Omega}_0^m}{\partial y} = 0, \tag{5.5}$$

and

$$\frac{\partial^2 \tilde{\psi}_0^n}{\partial y^2} - n^2 \tilde{\psi}_0^n = \tilde{\Omega}_0^n; \quad -N \leqslant n \leqslant N. \tag{5.6}$$

The numerical solution to this problem is obtained by marching in $\bar{x}$ from the initial condition (3.14) by the following procedure. The 'time-dependent' vorticity equation (5.5) is advanced in $\bar{x}$ by the midpoint leap-frog method which is marginally stable, non-dissipative and treats the nonlinear terms explicitly. The latter can therefore be efficiently calculated by inverse transforming to physical space, forming the products and then transforming back to Fourier space using a standard fast Fourier transform routine. In addition, only modes with $n \geqslant 0$ need to be calculated; the remaining modes are obtained by using (5.4). The updated vorticity is then used in the stream-function equation, where a second-order central difference approximation yields a tridiagonal system of equations for each Fourier component. The boundary condition (3.14) and (3.15) are imposed at the step. The velocity components are then evaluated from (3.9) and (3.10). One-sided differences are used to evaluate y-derivatives at the wall. The marching procedure is started by Heun's two-step method (Roache 1976, p. 88) which has the same order truncation error as the leap-frog method.

5.2. *Three-dimensional boundary-layer flow*

Numerical solutions to the three-dimensional boundary-layer problem (4.9)–(4.15) were obtained using a finite-difference scheme similar to the Keller box method used in I but with several important modifications to be discussed below.

To facilitate the numerical calculations, the problem is expressed in terms of the Blasius variable

$$\eta = \frac{\bar{y}}{\bar{x}^{\frac{1}{2}}}, \tag{5.7}$$

as a system of five first-order equations

$$p' + ep = \bar{x}\left[U\frac{\partial U}{\partial \bar{x}} + W\frac{\partial U}{\partial z}\right], \tag{5.8}$$

$$q' + eq = \bar{x}\left[U\frac{\partial W}{\partial \bar{x}} + W\frac{\partial W}{\partial z}\right] + \bar{x}\frac{\mathrm{d}P}{\mathrm{d}z}, \tag{5.9}$$

$$U' = p, \tag{5.10}$$

$$W' = q, \tag{5.11}$$

$$e' = \tfrac{1}{2}U + \bar{x}\left[\frac{\partial U}{\partial \bar{x}} + \frac{\partial W}{\partial z}\right], \tag{5.12}$$

where $' = \partial/\partial\eta$. The boundary conditions are given by (4.12)–(4.14) and

$$e(\bar{x}, \eta = 0, z) = 0. \tag{5.13}$$

The initial condition at $\bar{x} = 0$ is the Blasius solution.

Second-order finite-difference approximations are introduced in (5.8)–(5.12) in the same way as in I (see also Cebeci, Khattab & Stewartson 1981) except that the spanwise convection terms, i.e. $W\partial U/\partial z$ and $W\partial W/\partial z$, are replaced with a second-order upwind approximation (see, for example, Johnston 1990) in order to deal with the local regions of reverse cross-flow that occur in the boundary layer for this problem. The procedure advances the solution in the streamwise and spanwise directions from the initial condition at $\bar{x} = 0$ and an independent symmetry-plane solution, respectively. The symmetry planes, on which $W = 0$, are located at $z = 0$, π, 2π for our chosen upstream disturbance (see (6.1) below). Where possible we march from one symmetry plane to another in the direction of positive external spanwise velocity (from $z = \pi$ to 2π in our particular case). The first and last spanwise steps require special treatment. Since $\partial W/\partial z > 0$ along the initial symmetry plane (at $z = \pi$) the standard Keller box differencing can be used to start the spanwise marching. The upwind differencing is maintained at the last step (one grid point before the second symmetry plane) as long as $W > 0$ there, otherwise a central difference is used. Data on the second symmetry plane are available as a 'boundary condition' when needed.

Introduction of the finite-difference approximations yields a nonlinear system of algebraic equations for the unknown variables at the next (streamwise or spanwise) grid point. The latter are linearized by Newton's method and the resulting linear equations are solved with a block tri-diagonal algorithm. Each iteration consist of a single sweep across the span (from $z = \pi$ to 2π) at a new streamwise station and the solution is iterated to convergence for all z before proceeding downstream. Only a half-period of the flow needs to be calculated, the remainder can be obtained from symmetry.

6. Results and discussion

Our analysis shows how an initial streamwise vorticity distribution, imposed upstream of the leading edge, is converted, by linear processes, to a downstream vorticity distribution characterized by a cross-flow stream function ψ_0 which in turn

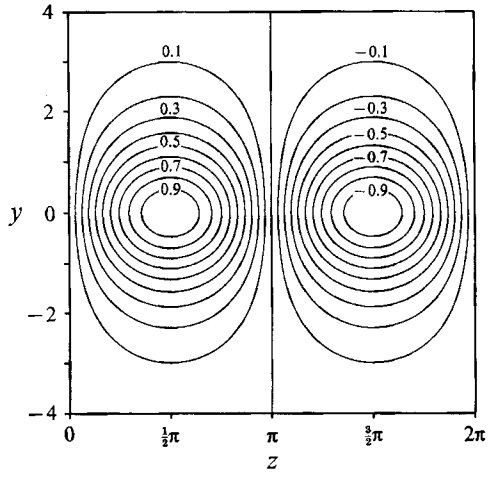

FIGURE 2. Streamline pattern in the cross-flow plane of the imposed steady upstream disturbance field.

provides the upstream boundary condition for the nonlinear inviscid problem discussed in the previous section.

For numerical purposes we have chosen the stream function of the imposed upstream flow to be

$$\psi_\infty(y,z) = \sin z \operatorname{sech} y. \tag{6.1}$$

It was selected because it is one of the simplest spanwise-periodic functions that exhibits exponential decay away from the plane of the plate. It represents an infinite array of counter-rotating streamwise vortices centred at the surface of the plate. The corresponding streamline pattern is shown in figure 2.

The downstream stream function ψ_0, which is easily obtained (2.6)–(2.7) by a linear Wiener–Hopf calculation (Noble 1958), is given

$$\psi_0(y,z) = \sum_{n=-\infty}^{\infty} \{\tilde{\psi}_\infty^n(y) - \tilde{\psi}_\infty^n(y=0)\,\mathrm{e}^{-|n|y}\}\,\mathrm{e}^{\mathrm{i}nz}, \tag{6.2}$$

where $\tilde{\psi}_\infty^n$ are the coefficients of the Fourier series expansion for ψ_∞. This was combined with the numerical procedure of §5.1 to calculate the nonlinear inviscid cross-flow streamline patterns shown in figure 3. These results show that the nonlinear inviscid flow above the plate consists of counter-rotating pairs of streamwise vortices. The counter-rotating vortex pairs move together by self-induction while they are close to the plane of the plate, causing the upwash velocity between the paired vortices to increase. However, this effect is eventually reversed as the paired vortices move away from the surface of the plate under the influence of their mutual induction fields. Unlike the nonlinear inviscid flow in I, where the upwash velocity becomes infinite at a finite downstream position, the upwash velocity remains bounded throughout the nonlinear region. This is due to the additional nonlinear and pressure gradient terms in the inviscid equations, particularly those in the spanwise momentum equation (3.7), which limit the growth of the upwash velocity.

While the qualitative behaviour of the inviscid flow field is relatively unremarkable, the viscous flow in the three-dimensional boundary layer beneath this inviscid region is much more interesting. The three-dimensional effects are driven by

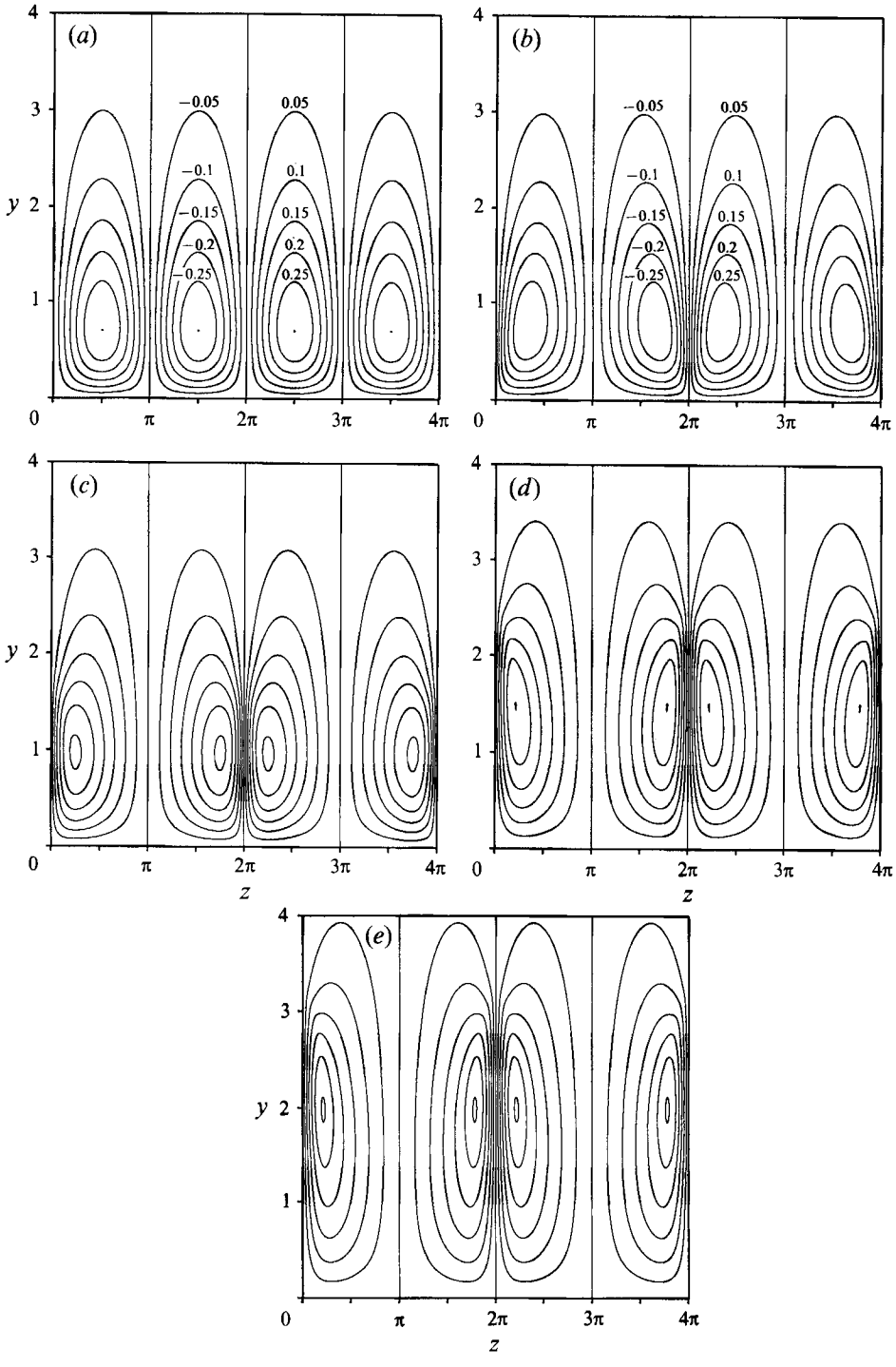

FIGURE 3. Evolution of the nonlinear, inviscid streamline pattern in the cross-flow plane. (*a*) $\bar{x} = 0$, (*b*) $\bar{x} = 2$, (*c*) $\bar{x} = 4$, (*d*) $\bar{x} = 6$, (*e*) $\bar{x} = 8$. Numbers indicate $\tilde{\psi}_0$ levels plotted.

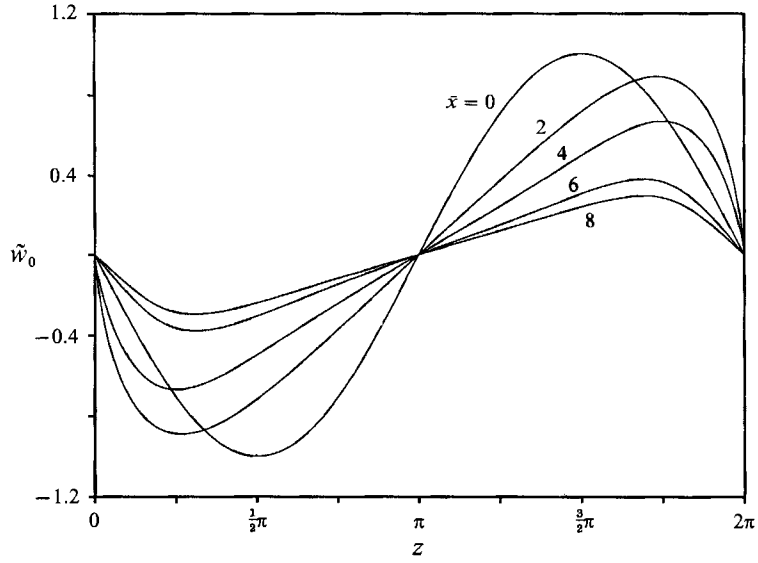

FIGURE 4. Inviscid cross-flow velocity at the surface of the plate.

the inviscid spanwise velocity and the pressure gradient at the plate surface. The former is plotted in figure 4. Notice that the maximum slope of the cross-flow velocity, which occurs at $z = 2\pi$, initially increases but is eventually reduced, along with the maximum amplitude of the cross-flow velocity, as the vortices move away from the plate when the scaled streamwise coordinate $\bar{x}$ exceeds about 2. This should be contrasted with the spanwise surface velocities in I where the spanwise gradient becomes infinite at a finite streamwise position and thereby drives the wall shear stress to zero in the induced boundary-layer flow.

Figure 5 shows the boundary-layer streamwise velocity contours in the cross-flow plane at the indicated streamwise positions. They show that the boundary layer undergoes a severe thickening around $z = 5.37$ and suggest that the solution begins to break down just downstream of $\bar{x} = 0.935$. These results are best understood by looking at the velocity vectors in the cross-flow plane shown in figure 6. This flow corresponds to the 'footprint' on the boundary layer of the large streamwise vortices that reside at an order-one distance from the wall. The figure shows that the rapid thickening of the boundary layer is due to a strong (nearly) vertical jet that is fed by the main vortex and a secondary vortex, having the opposite sense of rotation, that forms near the symmetry plane at $z = 2\pi$ (and $z = 0$) for $\bar{x}$ beyond about 0.4. The secondary vortex core moves away from the wall and towards the opposite symmetry plane (at $z = \pi$) with increasing downstream distance. The flow is not dissimilar to the two-dimensional time-dependent boundary-layer flow due to a pair of counter-rotating vortices above a plane wall calculated by Ersoy & Walker (1985, 1986). There also the production of secondary vortices precedes the boundary-layer breakdown with the latter occurring off the plane of symmetry. We note that this is contrary to the view that the motion induced by the vortices leads to symmetry-line boundary-layer collisions (Stuart 1988). It is worth noting that no secondary vortex is generated in the boundary-layer flow in I and the corresponding vertical jet therefore forms on the symmetry plane.

The jet increases in strength and decreases in width with increasing downstream distance and the spanwise velocity eventually becomes discontinuous across the jet

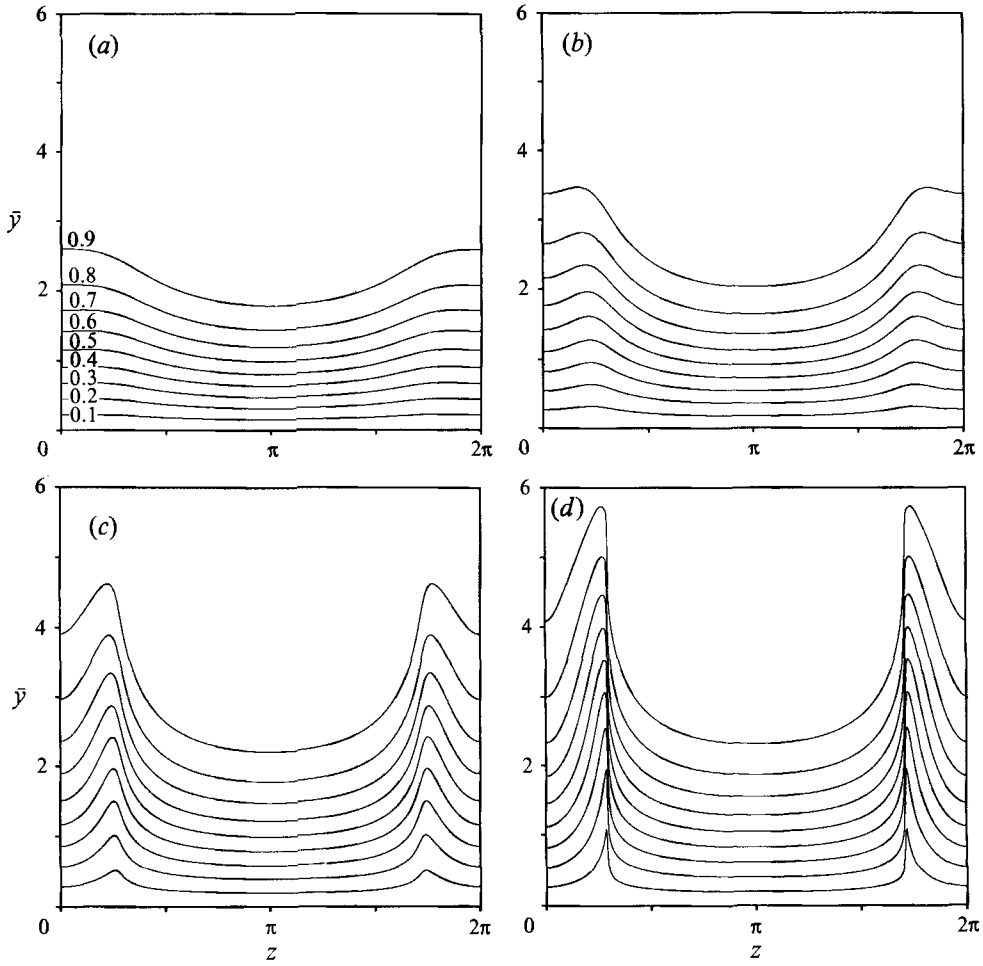

FIGURE 5. Boundary layer streamwise velocity contours in the cross-flow plane at (*a*) $\bar{x} = 0.4$, (*b*) $\bar{x} = 0.6$, (*c*) $\bar{x} = 0.8$, (*d*) $\bar{x} = 0.935$.

while the vertical velocity becomes infinite there. This, in particular, causes the so-called 'blowing velocity'

$$V_\infty = \lim_{\bar{y}\to\infty}\left\{V + \bar{y}\frac{\partial W}{\partial z}\right\}, \tag{6.3}$$

to also become infinite which is often taken as a separation criterion for three-dimensional boundary-layer flows. The spanwise blowing velocity distributions are plotted in figure 7. (Only half a period is shown here.) Extrapolation of our computed results indicates that the separation point occurs at $\bar{x} \approx 0.955$, $z \approx 5.37$.

Figure 8 is a plot of the streamwise and spanwise wall shear stress components as a function of z for various values of $\bar{x}$. The streamwise component (figure 8*a*) develops a very sharp minimum near the vertical jet position $z = 5.37$. The spanwise component (figure 8*b*) clearly shows the cross-flow reversal associated with the secondary vortex beginning near the $z = 2\pi$ symmetry plane at about $\bar{x} = 0.4$. The reverse cross-flow region then spreads out in the spanwise direction until it occupies more than one quarter of the spanwise domain just before the boundary layer

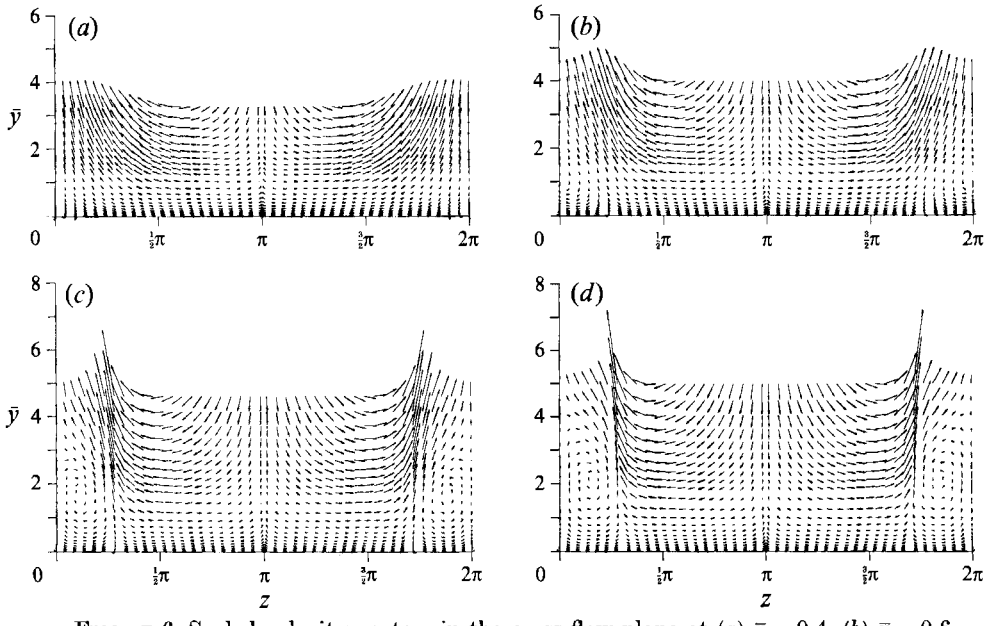

FIGURE 6. Scaled velocity vectors in the cross-flow plane at (*a*) $\bar{x} = 0.4$, (*b*) $\bar{x} = 0.6$, (*c*) $\bar{x} = 0.8$, (*d*) $\bar{x} = 0.935$.

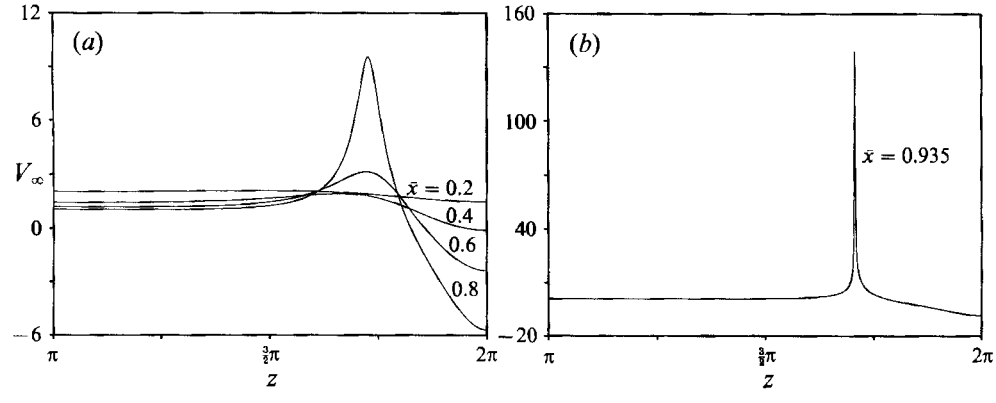

FIGURE 7. Blowing velocity *vs.* z at (*a*) $\bar{x} = 0.2$, 0.4, 0.6, 0.8 and (*b*) $\bar{x} = 0.935$.

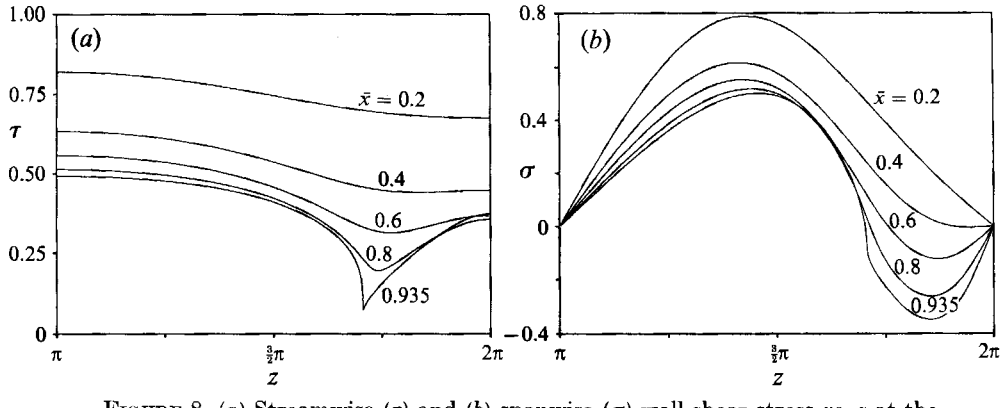

FIGURE 8. (*a*) Streamwise (τ) and (*b*) spanwise (σ) wall shear stress *vs.* z at the same streamwise locations as in figure 7.

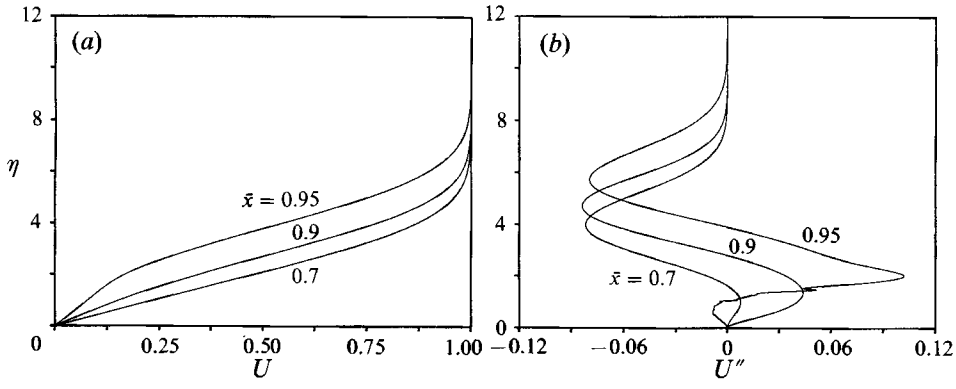

FIGURE 9. Development of (*a*) streamwise velocity profiles and (*b*) the corresponding second derivatives at $z = 5.37$ as the separation point is approached.

separates. Notice that, near the wall, the magnitudes of the maximum and minimum cross-flow velocities are almost equal by $\bar{x} = 0.935$.

Figure 6 suggests that the vertical jet is associated with the transport of low-momentum fluid away from the wall by the cross-flow vortices. Prandtl (1935) predicted that this redistribution of low-momentum fluid would have a significant effect on the streamwise velocity profiles – eventually causing them to become inflexional. Figure 9(*a*) shows the streamwise velocity profiles (*vs.* the Blasius variable η) at $z = 5.37$ for a number of streamwise positions up to the separation point. The results confirm that the profiles do indeed become inflexional, beyond about $\bar{x} = 0.6$. The inflexion points are more easily seen in figure 9(*b*) where the second derivatives of the corresponding profiles are shown. Note the existence of two inflexion points at $\bar{x} = 0.95$.

As Prandtl (1935) pointed out, this provides a possible mechanism for transition to turbulence since the inflexional profiles are quite unstable to inviscid Rayleigh instabilities whose wavelengths are of the order of the boundary-layer thickness and therefore short compared with the characteristic spanwise lengthscale (i.e. $\delta \ll 1$) so that the underlying mean flow is basically two-dimensional. Their growth rates will then be on the order of the reciprocal boundary-layer thickness and can therefore be much larger than those of the Tollmien–Schlichting waves, which are the primary instability of the undisturbed Blasius flow. We calculated the local spatial growth rates of the Rayleigh instabilities for the velocity profiles shown in figure 9. The results are shown in figure 10. The frequencies and growth rates are normalized by the boundary-layer thickness $\hat{\delta}$ corresponding to the position where the streamwise velocity is equal to 88 % of its free-stream value. This is done to facilitate comparison with the corresponding growth rates on a tanh shear layer, which is probably the most unstable of the generic model shear flows. Since the maximum spatial growth rate of the latter is equal to about 0.23 (Michalke 1965) the present flow must be regarded as highly unstable. Notice that the growth rates increase, while the unstable frequency band broadens and the peak growth rate shifts to higher frequency as the separation point is approached. This is primarily due to the movement of the inflexion point out from the wall as shown in figure 9*b*.

The regions of inviscidly unstable velocity profiles are highly localized in the spanwise direction. The rapidly growing instability waves could therefore lead to localized regions of turbulence perhaps taking the form of turbulent spots. The growth rates of the truly three dimensional instabilities associated with the spanwise

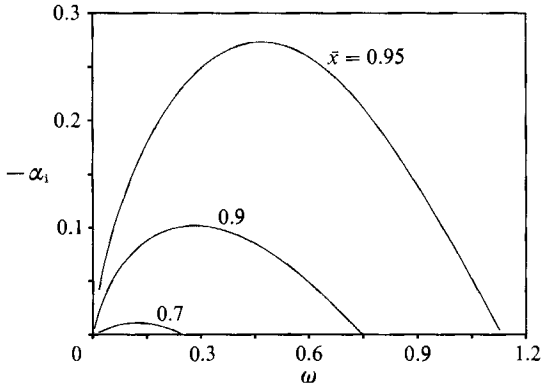

FIGURE 10. Normalized linear inviscid instability wave growth rates ($-\alpha_i$) *vs.* frequency (ω) for the velocity profiles in figure 9.

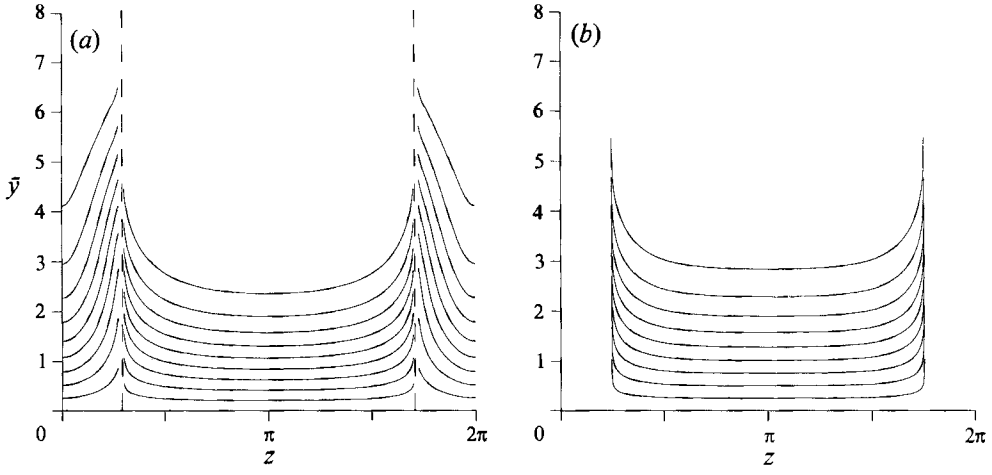

FIGURE 11. Streamwise velocity contours downstream of the initial separation point at (*a*) $\bar{x} = 1.0$ and (*b*) $\bar{x} = 2.0$. The levels plotted are the same as in figure 5. The dashed vertical line in (*a*) denotes the termination point of the numerical solution from the $z = \pi$ side.

flow variation scale with the inverse of the spanwise length scale λ and are therefore asymptotically smaller than the Rayleigh growth rates (which, as already noted, scale with $(\lambda\delta)^{-1}$)).

The numerical boundary-layer solution can be continued beyond the streamwise location, $\bar{x} = 0.955$, of the initial separation point provided the spanwise marching its terminated before we reach the location where the numerical solution breaks down. The terminal points trace out a curve, say $z_s(\bar{x})$, in the $(\bar{x}, z)$-plane that represents a boundary across which the numerical solution cannot be continued and may therefore correspond to a separation line. The flow on the other side of this line cannot, of course, be obtained by marching from the $z = \pi$ symmetry plane but must be computed by marching (against the free-stream flow) from the $z = 2\pi$ symmetry plane. The modifications to the numerical procedure needed to proceed are described in the Appendix. Unfortunately, this procedure, which is a development of the one introduced by Cebeci *et al.* (1981), is unable to calculate the complete flow field in the region $z_s < z \leqslant 2\pi$.

Figures 11 and 12 show the streamwise velocity contours and the cross-flow velocity vectors, respectively, at $\bar{x} = 1.0$ and 2.0. Figures 11 (*a*) and 12 (*a*) were constructed by

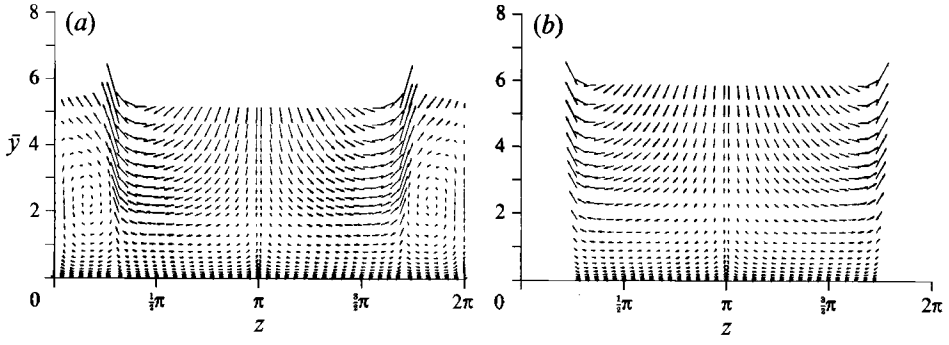

FIGURE 12. Velocity vectors in the cross-flow plane downstream of the initial separation point at (*a*) $\bar{x} = 1.0$ and (*b*) $\bar{x} = 2.0$.

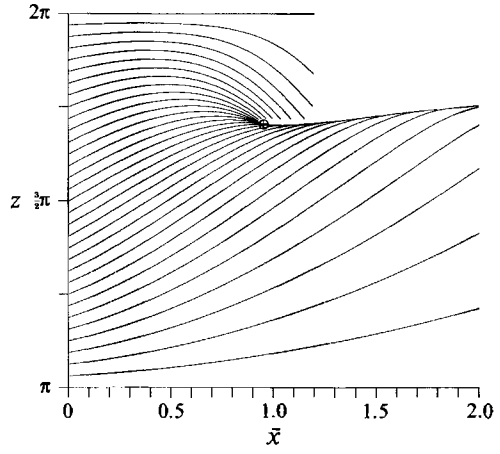

FIGURE 13. Limiting streamlines obtained from the boundary-layer calculation. ⊕ indicates position of blowing velocity singularity.

combining the $\bar{x} = 1.0$ solution initiated from the $z = \pi$ symmetry plane with the one initiated from the $z = 2\pi$ symmetry plane. The dashed line in figure 11 (*a*) marks the termination point of the marching from $z = \pi$. We only show the solution for $\pi < z < z_s$ in parts (*b*) of these figures because solutions between $z = z_s$ and $z = 2\pi$ could not be obtained at $\bar{x} = 2.0$. The results show that the cross-flow patterns downstream of the initial separation point remain very similar to the upstream patterns – the primary difference being a shift towards $z = 2\pi$ of the spanwise location of the termination point.

Figure 13 shows the surface (or limiting) streamlines, which are solutions of

$$\mathrm{d}\bar{x}/\mathrm{d}t = \tau, \quad \mathrm{d}z/\mathrm{d}t = \sigma, \tag{6.4}$$

where τ and σ are, respectively, the numerically computed streamwise and spanwise components of the wall shear stress. Lighthill (1963, p. 74) argued that the running together of neighbouring surface streamlines is a sufficient condition for three-dimensional boundary-layer separation. Figure 13 shows that the calculated surface streamlines merge at the extrapolated position of the blowing velocity singularity ($z = 5.37$, $\bar{x} = 0.955$) which is marked by ⊕ on the figure. This point may correspond to an isolated singular point (perhaps a saddle point) of the type proposed by Lighthill (1963) (see also the discussion in Cebeci *et al.* 1981).

The streamlines originating from the $z = \pi$ side of the initial singularity coalesce along a curve in the $(\bar{x}, z)$-plane which we identify with a separation line. The numerical procedure had to be modified in order to calculate this curve due to its drift towards $z = 2\pi$ with increasing $\bar{x}$ (see Appendix). The flow in this region is similar to that on the windward side of the flow of Cebeci *et al.* (1981) and we therefore expect that the wall shear stress distribution will be more or less consistent with the generalized Goldstein singularity postulated by Brown (1965). Of course the whole flow structure could change radically if a classical separation actually occurred. However, we can always suppose that the plate is short enough so that the separation lies off its end. Moreover, the highly unstable velocity profiles will almost certainly lead to boundary-layer transition upstream of the separation point, even when this is not the case.

As already indicated, we were unable to obtain as complete a picture of the other side of $z = z_s(\bar{x})$. In fact the condition of Raetz (1957) on the zone of dependence makes $z = z_s(\bar{x})$ inaccessible to our numerical scheme (Cebeci *et al.* 1981) from $z = 2\pi$. Figure 13 shows that the streamlines on the $z = 2\pi$ side of the initial singularity show no sign of turning to merge with $z = z_s(\bar{x})$ but rather appear to collide with this curve, which then represents the only separation curve for the flow. The increasing difficulty in obtaining solutions on the $z = 2\pi$ side (even on the symmetry plane) suggests that the separation curve will eventually run into the $z = 2\pi$ symmetry plane but the shape of this curve suggests that this will only occur very far downstream.

Several years ago Rozhko & Ruban (1987) proposed a scheme for weakly three-dimensional vortex-like flows which corresponds to the special scaling $\epsilon = R^{-\frac{3}{7}}$. Their approach involves a local three-dimensional interactive boundary-layer solution which, in the limit of zero curvature, is a limiting form of the conventional triple-deck structure. It is induced by a three-dimensional scaled surface non-uniformity and produces a faster streamwise response than the present approach. In the present problem the three-dimensional boundary-layer flow is induced by three-dimensional effects in the free stream, which are constrained by the imposed upstream flow to be $O(\epsilon)$. The free-stream velocity field in the Rozhko & Ruban (1987) analysis is much larger, $O(R^{\frac{1}{14}}\epsilon)$, and therefore cannot match onto the free-stream flow in the present analysis, which ultimately means that it cannot match with the imposed upstream conditions. In other words, the free-stream disturbances in the present analysis are unable to provoke a strong enough response within the boundary layer to produce the Rozhko & Ruban (1987) scaling. However, the larger free-stream velocities might be acceptable in some local region if they were forced by an internal mechanism within the boundary layer such as a global self-induced boundary-layer separation. The breakdown of the three-dimensional boundary-layer solution in the present analysis suggests that such a separation could occur if the plate were sufficiently long and transition did not occur upstream – which is unlikely to be the case in the present flow. In any event, the Rozhko & Ruban (1987) solution would then correspond to a local solution that was somehow embedded in a global solution of the type considered herein.

7. Concluding remarks

It has long been known that streamwise vortices are a pervasive feature of transitioning boundary-layer flows. Their importance was first realized by Prandtl (1935) and it has recently been suggested (for example, by Blackwelder 1983) that they may be a universal feature of both turbulent and transitional boundary layers.

They may even be responsible for producing the violent local events such as turbulent spots in the transitional case and bursts in the turbulent case.

Benney & Lin (1960) and Benney (1964) pointed out that steady streamwise vortices can result from the nonlinear interaction between spatially growing Tollmien–Schlichting waves. Here, we suggest that small-amplitude distortions of the upstream flow may provide another source of steady streamwise vortices within the flat-plate boundary layer. These vortices may allow the boundary layer to 'bypass' the linear Tollmien–Schlichting wave stage of transition and proceed directly to the much more rapidly growing inviscid instabilities associated with regions of nonlinear streamwise vortices. Since the unstable regions are highly localized in the spanwise direction, the initial region of turbulence would also be localized and might closely resemble the turbulent spots observed in some transition experiments.

Our results show that the upstream distortion will ultimately cause the boundary layer to separate if transition does not occur first.

The authors would like to thank Professor M. T. Landahl for reminding them of the leading-edge singularity in the linear inviscid solution of §2.

Appendix

This appendix describes the modifications that were made to the numerical procedure of §5.2 in order to advance the boundary-layer solution downstream of the initial separation point. It is essential that the proper zone of dependence be maintained in constructing the numerical schemes.

A.1. *Termination of the boundary-layer solution in the spanwise direction*

The finite differencing for the spanwise derivatives must be modified at the last two spanwise points when the boundary-layer solution is terminated before reaching a symmetry plane. We use upwind differencing whenever the sign of the local cross-flow velocity allows. Otherwise, a central difference is used for the penultimate grid point and the so-called zigzag scheme described by Cebeci *et al.* (1981) is used for the last point.

The shape of the separation curve is such that it is sometimes necessary to take one more spanwise step at a given streamwise station beyond what was taken at the previous streamwise position. We briefly describe the method devised to do this. The differential equations are centred as in the standard Keller box method (Cebeci *et al.* 1981) but values at the centre of the box are obtained as averages of the last spanwise grid points at the two streamwise stations. Upwind differencing is used for the spanwise derivatives and central differences are used for the cross-stream and streamwise derivatives (linear extrapolation at the previous streamwise station is also needed for the latter). In practice this scheme was used when it was thought that the separation curve cut through the bottom face of the lower-most finite-difference box, leaving one corner inside the separated region.

A.2. *Marching against the external cross-flow velocity direction*

The flow in the region $\bar{x} > 0.955$, $z_s(\bar{x}) < z < 2\pi$ must be calculated by marching from the symmetry plane at $z = 2\pi$ towards z_s. This requires a numerical procedure that is capable of marching against the external cross-flow direction. We tested the ability

of our upwind scheme to march in this direction by re-computing the solution in the region upstream of the initial separation point from the symmetry plane at $z = 2\pi$ and marching to the one at $z = \pi$. It was found that the solution obtained in this way was, to within the tolerance imposed, identical to that obtained by marching from the $z = \pi$ symmetry plane when the same numerical parameters (step sizes, etc.) were used. We therefore used the same upwind to march from $z = 2\pi$ towards $z_s(\bar{x})$, modifying only the end points. At the first spanwise grid point (from the $z = 2\pi$ symmetry plane) upwind or central differences were used for the spanwise derivatives, depending on the sign of the local spanwise velocity. When this spanwise marching is terminated, at say $z = z_t$, information is always required from $z < z_t$. At this point we used the zigzag differencing mentioned above. We used a central difference at the penultimate spanwise grid point where there are not enough points to do the upwind differencing if $W > 0$. As before, the upwind difference is used whenever possible. Upon convergence of the solution in $z_t < z < 2\pi$ data at $z_t - \Delta z$ were generated by linear extrapolation for use by the zigzag scheme at the next streamwise station (Cebeci & Su 1988).

REFERENCES

Benney, D. J. 1964 Finite amplitude effects in an unstable boundary layer. *Phys. Fluids* **7**, 319–326.

Benney, D. J. & Lin, C. C. 1960 On the secondary motion induced by oscillations in shear flow. *Phys. Fluids* **3**, 656–657.

Blackwelder, R. F. 1983 Analogies between transitional and turbulent boundary layers. *Phys. Fluids* **26**, 2807–2815.

Brown, S. N. 1965 Singularities associated with separating boundary layers. *Phil. Trans. Roy. Soc.* A**257**, 409–444.

Cebeci, T., Khattab, A. A. & Stewartson, K. 1981 Three-dimensional laminar boundary layers and the ok of accessibility. *J. Fluid Mech.* **107**, 57–87.

Cebeci, T. & Su, W. 1988 Separation of three-dimensional laminar boundary layers on a prolate spheroid. *J. Fluid. Mech.* **191**, 47–77.

Crow, S. C. 1966 The spanwise perturbation of two dimensional boundary layers. *J. Fluid Mech.* **24**, 153–164.

Ersoy, S. & Walker, J. D. A. 1985 Viscous flow induced by counter-rotating vortices. *Phys. Fluids* **28**, 2687–2698.

Ersoy, S. & Walker, J. D. A. 1986 Flow induced at a wall by a vortex pair. *AIAA J.* **24**, 1597–1605.

Goldstein, M. E. 1978 Unsteady vortical and entropic distortions of potential flows round arbitrary obstacles. *J. Fluid Mech.* **89**, 433–468.

Goldstein, M. E. 1983 The evolution of Tollmien–Schlichting waves near a leading edge. *J. Fluid Mech.* **127**, 59–81.

Goldstein, M. E. 1985 Scattering of acoustic waves into Tollmien–Schlichting waves by small streamwise variations in surface geometry. *J. Fluid Mech.* **154**, 509–529.

Goldstein, M. E., Leib, S. J. & Cowley, S. J. 1987 Generation of Tollmien–Schlichting waves on interactive marginally separated flows. *J. Fluid Mech.* **181**, 485–517.

Goldstein, M. E., Leib, S. J. & Cowley, S. J. 1992 Distortion of a flat plate boundary layer by free-stream vorticity normal to the plate. *J. Fluid Mech.* **237**, 231–260 (referred to herein as I).

Goldstein, M. E., Sockol, P. M. & Sanz, J. 1983 The evolution of Tollmien–Schlichting waves near a leading edge. Part 2. Numerical determination of amplitudes. *J. Fluid Mech.* **129**, 443–453.

Hall, P. 1988 The nonlinear development of Görtler vortices in growing boundary layers. *J. Fluid Mech.* **193**, 243–266.

HALL, P. 1990 Görtler vortices in growing boundary layers: the leading edge receptivity problem, linear growth and the nonlinear breakdown stage. *Mathematica* **37**, 151–189.

HALL, P. & HORSEMAN, N. J. 1991 The linear inviscid secondary instability of longitudinal vortex structures in boundary layers. *J. Fluid Mech.* **232**, 357–375.

HUNT, J. C. R. & CARRUTHERS, D. J. 1990 Rapid distortion theory and the 'problems' of turbulence. *J. Fluid Mech.* **212**, 497–532.

JOHNSTON, L. J. 1990 An upwind scheme for the three dimensional boundary layer equations. *Intl J. Numer. Meth. Fluids* **11**, 1043–1073.

LIGHTHILL, M. J. 1963 In *Laminar Boundary Layers* (ed. L. Rosenhead), p. 74. Dover.

MICHALKE, A. 1965 On spatially growing disturbances in an inviscid shear layer. *J. Fluid Mech.* **23**, 521–544.

NOBLE, B. 1958 *Methods Based on the Wiener–Hopf Technique for the Solution of Partial Differential Equations.* Pergamon.

PRANDTL, L. 1935 *Aerodynamic Theory.* Springer.

RAETZ, G. S. 1957 A method of calculating three dimensional boundary layers of compressible flows. *Northrop Corp. Rep.* NAI 58-73.

ROACHE, P. J. 1976 *Computational Fluid Dynamics.* Hermosa.

ROZHKO, S. B. & RUBAN, A. I. 1987 Longitudinal–transverse interaction in a three dimensional boundary layer. *Fluid Dyn.* **23**, 362–371.

STEWARTSON, K., CEBECI, T. & CHANG, K. C. 1980 A boundary layer collision in a curved duct. *Q. J. Mech. Appl. Maths* **33**, 59–75.

STEWARTSON, K. & SIMPSON, C. J. 1982 On a singularity initiating a boundary layer collision. *Q. J. Mech. Appl. Maths* **35**, 1–16.

STUART, J. T. 1988 Nonlinear Euler partial differential equations: singularities in their solution. In *Proc. Symp. Honor of C.C. Lin* (ed. D. J. Benney, Chi Yuan, F. H. Shu), pp. 81–95. World Scientific.